JOURNAL OF PROPULSION AND POWER
Vol. 27, No. 4, July–August 2011

Numerical Study of Erosive Burning in Multidimensional Solid Propellant Modeling

Victor D. Topalian,* Ju Zhang,† Thomas L. Jackson,‡ and Amir H. G. Isfahani§
University of Illinois at Urbana–Champaign, Urbana, Illinois 61801

DOI: 10.2514/1.B34090

Using numerical simulations, the combustion response of heterogeneous solid propellants to an imposed crossflow velocity field are examined. It is shown that this model flow is useful to capture the influence of shear flow in the so-called erosive burning phenomenon observed in actual experiments. Previous numerical studies on a model quarter-plane problem and on homogeneous solid propellants have shown that the presence of shear in the crossflow plays a role in increasing the heat transfer to the propellant surface, thus enhancing the burn rate. In the current work, the response of two- and three-dimensional packs to an imposed velocity field are first examined for different propellant morphologies and at different pressures. The imposed velocity field has its root in a separate nonreactive multiscale analysis. It is shown that, with the model flow, the variations of the erosive burning rate with shear parameters are captured, the trends being in line with experimental results. Furthermore, a comparison with experimental results present in the literature is examined, where it is shown that the results compare qualitatively well with the experiments using the estimated shear rates from the experiment. These results suggest that the influence of the shear flow on the primary diffusion flame may be a leading factor in the erosive burning effect.

I. Introduction

EROSIVE burning is the variation of the local burn rate of a solid propellant from its strand value that occurs in the presence of a crossflow velocity. The burning rate in the presence of crossflow may either increase or decrease from the nominal burn rate: situations referred to as positive or negative erosion, respectively.

For composite solid propellants, erosive burning was first reported by Green [1] and, subsequently, in a number of independent studies and review articles [2–12]. Experimental results show that, in general, the nominal burn rate increases with increasing crossflow velocity. For ammonium perchlorate/hydroxyl-terminated polybutadiene (AP/HTPB) propellants, the erosive burning rate depends on the coarse-grain AP diameter, type of binder, and temperature in the unburnt propellant, although it is not sensitive to crossflow temperature, crossflow composition, and metal addition.

A number of mechanisms have been proposed to explain erosive burning of composite propellants [6,9–11,13]. It is generally argued that the crossflow affects the heat transfer from the gas phase to the surface, affecting temperature and the rate at which the propellant evaporates. It has been proposed that the source of this heat transfer is either the heat increase in the flow due to velocity increase, the bending of the final diffusion flame toward the propellant surface, or the increase in thermal conductivity and the diffusion coefficients in the gas phase due to turbulence. As a result, a number of empirically based models have been developed (e.g., Lenoir and Robillard [14]), but none of them fit all the data. There is a need for better understanding of the physical phenomena at the solid propellant combustion scale that can produce erosive burning.

In the current work, we study, by numerical simulations, the effects of an imposed shear flow on the burning rate of two- and three-dimensional AP/HTPB propellant packs. We consider different mean particle diameters for both two- and three-dimensional packs. The mean particle diameters of AP are taken to be 90 and 200 μm in the two-dimensional study and 90, 200, and 400 μm in the three-dimensional study. The packs are subjected to different shear rates and at different pressures. This range of parameters allows us to study the erosive burning effect caused by the imposed shear flow at different pressures and shear rates. It also allows us to account for the grain size effect that is evident in experiments. As a result, the trends observed are in agreement with experimental observation [6], with higher burn rates observed as the shear rate increases and an increased erosive burning rate coefficient obtained for packs with particles of higher mean diameter.

These results are consistent with the explanation of the quarter-plane geometry [15,16], where it was shown that when binder gases are blown over the AP particle, the area over which the primary diffusion flame (PDF) is significant increases (located over the AP particle, a consequence of the location of the Burke–Schumann flame sheet model [17,18]). Therefore, decreasing the AP particle diameter effectively decreases the area over which the PDF is significant, thereby decreasing the erosive burning effect.

Another set of three-dimensional simulations is performed in order to compare the numerical results with those obtained experimentally. This is achieved by considering a bimodal pack of AP/HTPB, composed of AP particles of mean diameters of 200 and 90 μm, with the mass fraction of each cut 68.35 and 13.65%, respectively. Results for a propellant of similar characteristics were reported by King [6]. It is shown that there is good agreement between the trends in experimental and numerical results, after considering an order of magnitude estimate of the shear rate in the experiments by King.

The present work is structured as follows. In Sec. II, the main findings of previous numerical studies are summarized, and the implications of those findings for the modeling of erosive burning is discussed. In Sec. III, the model for the combustion of AP/HTPB used in the present study is outlined. In Sec. IV, the results of the simulations for the selected two- and three-dimensional packs are presented, and in Sec. V, the results and discussion of the packs used to compare with experiments are presented.

Presented as Paper 2010-6903 at the the 46th AIAA/ASME/SAE/ASEE Joint Propulsion Conference and Exhibit, Nashville, TN, 25–28 July 2010; received 19 August 2010; revision received 1 January 2011; accepted for publication 3 January 2011.

*Postdoctoral Research Associate, Computational Science and Engineering; topalian@illinois.edu. Member AIAA.

†Research Scientist, Computational Science and Engineering; juzhang@illinois.edu. Senior Member AIAA (Corresponding Author).

‡Senior Research Scientist, Computational Science and Engineering; tlj@illinois.edu. Associate Fellow AIAA.

§Research Assistant, Department of Mechanical Science and Engineering; ghalayan@illinois.edu. Member AIAA.

II. Summary of Previous Numerical Studies

The erosive burning effect was studied recently with the aid of numerical simulations on model problems. In the context of solid rocket motors (SRMs), it is not possible, to date (due to computational limitations), to study erosive burning using direct numerical simulations (DNSs) for the coupled problem of the flowfield in the rocket chamber and the burning of the solid propellant. However, numerical studies have been conducted separately, using different frameworks, both on the SRM flowfield [19,20] and on the burning of solid propellants subjected to an imposed velocity field [15,16,21].

The studies on the flowfield allowed to characterize turbulence in the rocket motor: in particular, very close to the burning surface. In this regard, they provide data to estimate the magnitude and frequency of the shear rate and velocity fluctuations, which are relevant for the erosive burning effect. Similarly, the studies on the burning of solid propellants subjected to an imposed velocity field allowed us to numerically evaluate the burning response of solid propellants in the presence of shear flow. The main findings of these studies using numerical simulations on model problems are summarized next.

A. Studies on Velocity Fluctuations

1. *Multiscale Analysis for Rational of Assigned Velocity Field*

The crossflow that produces the erosive burning effect generates an unsteady shear flow near the propellant surface, which affects the combustion and the heat flux to the propellant. To evaluate the effects of these velocity fluctuations in the combustion of solid propellants in actual rocket chambers, it is of interest to have an estimate of the magnitude of such fluctuations. Computationally, such estimates can be obtained through the use of a multiscale formulation, which makes it possible to perform a DNS of the flowfield at different axial stations or positions in the rocket chamber.

The multiscale analysis is based on the assumption that both the mean flow and the rms velocities evolve slowly in the streamwise direction, with the turbulent fluctuations evolving on the fast scale. This has been formulated by Spalart for turbulent boundary layers [22]. Venugopal et al. [19] extended it to three-dimensional injection-driven plane channel flows as a model for planar SRM simulations. Zhang and Jackson [20] applied the formulation to cylindrical geometries for incompressible flow, which is expected to be a reasonably good approximation for low Mach number flows for center-perforated SRMs.

For the multiscale analysis, a "slow" ($x_s = \epsilon x$) variable and a "fast" ($x_f = x$) variable are introduced in the streamwise direction, where ϵ is a small parameter. Within the SRM context, ϵ determines the flow dynamics at any plane with streamwise location $X/h = 1/\epsilon$, where X is the distance from the head end, and h is the half-width (radius) of the chamber for a planar (cylindrical) geometry. The variable ϵ is also the ratio of mass injection rate to the mean flow rate at the streamwise location X [19]. For more details of the formulation and the numerical scheme, the interested reader is referred to the original works [19,20].

2. *Model of Velocity Field Near Propellant Surface*

The results of the multiscale study of Zhang and Jackson [20] suggest that, near the propellant surface, there are strong velocity gradients that have both a quasi-periodic temporal dependence and a quasi-periodic spatial structure. We therefore model the velocity field near the surface for a planar geometry, for example, as

$$u = A\cos\left(\frac{2\pi}{\lambda}x\right)\sin(\omega t)y \tag{1a}$$

$$v = v_{\text{inj}} + \frac{A\pi}{\lambda}\sin\left(\frac{2\pi}{\lambda}x\right)\sin(\omega t)y^2 - \frac{A}{2}\epsilon\cos\left(\frac{2\pi}{\lambda}x\right)\sin(\omega t)y^2 \tag{1b}$$

Here, v_{inj} (cm $\cdot$ s^{-1}) is the injection velocity at the propellant surface: $\omega = 2\pi f$ with f (Hz) being the frequency; $A(s^{-1})$ is the shear amplitude; and λ (cm) is the wavelength. Note that even though this velocity field is assigned for a planar geometry, it is relevant near the propellant surface and adequate for erosive burning modeling. The third term on the right-hand side of Eq. (1b) for v arises so as to satisfy the continuity equation in the multiscale formulation; that is,

$$\frac{\partial u}{\partial x_f} + \epsilon\frac{\partial u}{\partial x_s} + \frac{\partial v}{\partial y} = 0 \tag{2}$$

If the third term of Eq. (1b) is zero, then the assigned velocity field is solenoidal. Results suggest that the third term has little effect on the erosive burning characteristics, and so whether one keeps the term or not is only a matter of preference. Also, note that x in Eq. (1) is equivalent to x_f in the multiscale formulation and the slow derivative terms $\frac{\partial u}{\partial x_s} = u$ in the multiscale formulation are a modeled term [20].

The wavelength λ in Eq. (1) determines the axial (i.e., tangential) spatial structure of the imposed velocity field. It has been shown [21] that the wavelength is on the order of a millimeter, possibly too large to have an effect on heterogeneous propellants (with the size of the particles on the order of microns), yet it can have an effect on homogeneous propellants. Then, for modeling the flowfield for heterogeneous propellants, we take the limit of $\lambda \to \infty$ and ignore the x-spatial structure, and the imposed velocity field reduces to Eq. (8) later. For homogeneous propellants, we keep the x-spatial dependence but ignore the time dependence because of the difference in magnitude between the characteristic time scales associated with the combustion sublayer and the chamber flow. Since the dominant shear frequencies are typically 100–1000 Hz [20] for most motors and the reference frequency in the flame simulation is $\sim 1 \times 10^5$ Hz, a nondimensional frequency ω of less than 0.01 seems to be a reasonable value. Therefore, the imposed velocity field can be viewed as quasi steady. Note that the preceding simplifications are made solely for the purpose of clarifying whether it is the spatial or temporal structures that matters more. One could, of course, discard the preceding simplifications and impose the velocity field given by Eq. (1) for all the erosive burning simulations, regardless of homogeneous or heterogeneous propellants. The results and conclusions are either expected or confirmed to remain essentially the same as those with the simplifications.

3. *A Priori Estimate of Importance of Erosive Burning*

The results from the multiscale analysis can be used to obtain an a priori estimate of the importance of erosive burning for a given motor geometry. We highlight and discuss, in this section, the procedure to obtain such an estimate.

Figure 1a is a plot of the nondimensional shear at the burning surface versus the maximum crossflow velocity for different positions in the rocket chamber, a main result from the multiscale analysis [20]. To obtain these results, the multiscale problem was solved for each value of ϵ; therefore, the mean nondimensional velocity at the centerline $U_{\max}$ and the total mean nondimensional shear (mean plus rms) at the surface were determined. The shear rate is defined as the velocity gradient in the wall-normal direction at the injection surface, where the streamwise velocity used is one point away from the surface and the velocity is assumed to have a linear profile down to the surface. The figure thus shows a universal relationship between the crossflow velocity and shear for a single Re_{inj} of 1000. It was determined, however, that the shear amplitude shows only a weak dependence on Re_{inj}, especially for large values of Re_{inj}. For example, for ϵ of 0.04, the total shear (mean plus rms) for $Re_{\text{inj}} = 1000$ is only 17% smaller than that for $Re_{\text{inj}} = 5000$, and it is 20% smaller than that for an inviscid solution.

The relationship shown in Fig. 1a can now be tailored for a particular rocket chamber; therefore, one can obtain an estimate of the shear rate, which allows us to determine a priori the importance of erosive burning for a given motor geometry.

An illustration of this process is described next, where the rocket parameters used are listed in Table 1 and the final results are shown in Fig. 1b. This figure plots the magnitude of the shear rate versus maximum velocity for each rocket considered in Table 1, where the reference scales necessary for calculating dimensional values from

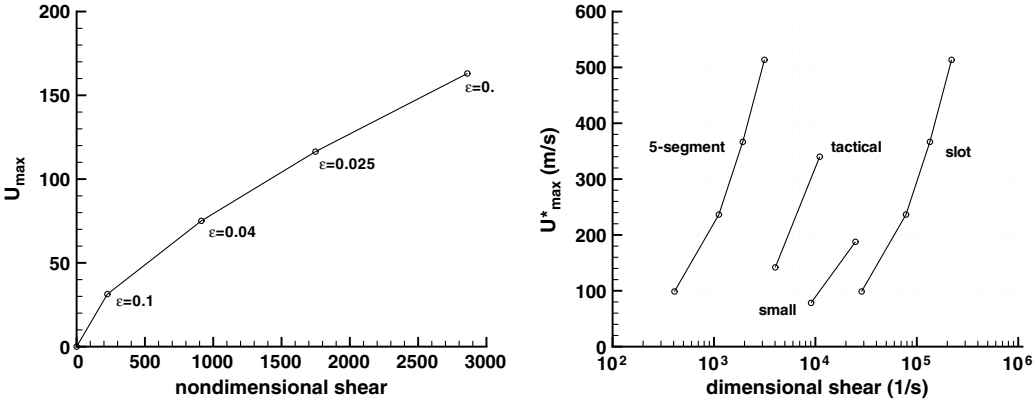

Fig. 1 Plots of a) nondimensional crossflow velocity as a function of nondimensional shear rate for $Re_{\text{inj}} = 1000$; and b) dimensional crossflow velocity as a function of dimensional shear rate for a variety of motor geometries.

nondimensional multiscale analysis solutions are given. In particular, h is the length scale, v_{inj} is the velocity scale, and v_{inj}/h is the shear amplitude scale. In the curve for each rocket, the axial location is found from the relation $X = h/\epsilon$. Thus, the value corresponding to the smallest crossflow velocity corresponds to an axial location near the head end, while the largest crossflow velocity corresponds to an axial location near the aft end. For example, for the small motor, there are only two points plotted that correspond to $\epsilon = 0.1$ and 0.04, giving axial locations of $X = 0.25$ and 0.625 m, respectively, with the last value roughly corresponding to the aft end of the motor. We comment that Fig. 1b can be used as well for determining a priori the importance of erosive burning when only the crossflow velocities, but not the shear rates, are measurable and available in rocket design process.

Regarding the data for each rocket considered in Table 1, the relevant ranges of the injection Reynolds number given are for typical operating conditions with a temperature range of 2400–3000 K and a pressure range of 10–100 atm. In obtaining these ranges, we assume that the propellant burn rate follows the empirical relation with pressure:

$$r_b = aP^n \tag{3}$$

The injection velocity can be obtained by the connection condition across the solid–gas interface through

$$v_{\text{inj}} = (\rho_c - \rho_g) r_b/\rho_g \approx \rho_c aRT/P^n \tag{4}$$

The kinematic viscosity ν is obtained using

$$Pr = \frac{\nu}{\kappa} \tag{5}$$

where Pr is the Prandtl number and $\kappa = \lambda_g/\rho_g c_p$ is the thermal diffusivity, with the thermal conductivity λ_g (in $\text{W} \cdot \text{m}^{-1} \cdot \text{K}^{-1}$), given by

$$\lambda_g = 1.08 \times 10^{-4} T + 0.0133 \tag{6}$$

To compute the values given in the Table 1, we used $a = 0.14\ \text{cm} \cdot \text{s}^{-1} \cdot \text{atm}^{-0.5}$, $n = 0.5$, and $Pr = 0.72$, with the value of a obtained from Massa et al. [23]. The dimensional frequency range, at the head to the aft end, are for typical nondimensional frequencies of about 10, 50, 80, and 100, corresponding to ϵ of 0.1, 0.04, 0.025, and 0.017, respectively, based on the results from the multiscale simulations [20].

4. *Estimate of Near-Wall Eddy Viscosity*

A thorough discussion regarding the characteristics and estimates of the near-wall shear can be found in the original work by Zhang and Jackson [20]. In this section, we use those results to obtain an estimate of the turbulent eddy viscosity near the surface, which has been widely used in the rocket propulsion community as a parameter in erosive burning modeling. We will show that, according to the results from the multiscale simulations, the turbulent eddy viscosity is smaller near the surface than what is generally assumed; hence, the use of turbulent transport modeling in models of erosive burning might need to be reevaluated.

King [6] (and references therein) assumes that the total (molecular plus turbulent) thermal conductivity can be written as

$$\frac{\lambda_t}{\lambda_L} = 1 + \frac{\nu_t}{\nu_L} = 1 + \frac{0.168X^2(DF)^2 \text{d}u/\text{d}x}{\nu_L} \tag{7}$$

where X is the distance from the propellant surface and DF is the damping factor. The expression for ν_t in the preceding equation is based on Prandtl's mixing length theory for an incompressible boundary layer (nontranspired flows). Note the X^2 dependence of the turbulent viscosity on the distance from the surface. In Fig. 2, we plot ν_t/ν_L as a function of distance from the surface for different injection Reynolds numbers obtained from the multiscale analysis results [20] for an ϵ of 0.04 three-dimensional cylindrical multiscale simulation; the reference length scales are $h = 2.5$ cm (top x axis; appropriate for small rocket) and $h = 0.7$ m (bottom x axis; appropriate for space shuttle). Also shown in Fig. 2 are the X^2 form assumed by King [6] and the slope (dotted–dashed curve) that is obtained from the multiscale analysis $X^{3.5}$. It is seen that the formula used by King overestimates the turbulent eddy viscosity near the surface. This might explain why heuristic formulas, such as Eq. (7), can be calibrated for one set of experimental data yet fails for other data sets.

As a final comment, we note that in Isfahani et al. [16], it was demonstrated that the PDF is of leading importance on the overall

Table 1 Parameters for typical motors of different sizes

Parameter	Small	Tactical	Space shuttle	Slot
Radius h, m	0.025	0.102	0.700	0.01
Length L, m	0.6	2.03	41.0	1.0
Injection velocity v_{inj}, $\text{m} \cdot \text{s}^{-1}$	2.5024	4.5322	3.1487	3.1487
Frequency f, Hz	[1e − 3, 5e − 3]	[453, 2265]	[45, 360]	[3149, 3.15e − 4]
Injection Reynolds number $Re_{\text{inj}} = v_{\text{inj}}h/\nu$	[700,3000]	[3000, 1e − 4]	[1e − 4, 1e − 5]	[300,1000]

[a]Numbers in brackets correspond to extreme values of temperature range from 2400–3000 K and to pressure range of 10–100 atm.

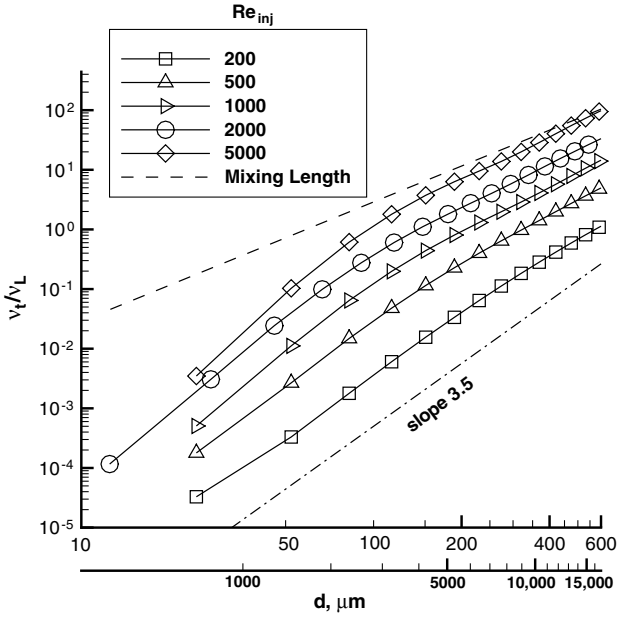

Fig. 2 Ratio of turbulent to laminar viscosity of flows with transpired walls as a function of distance from the wall, $d = 1 - r$.

burning rate and may be a main factor in the erosive burning effect. Since the location of the PDF lies within 10–30 μm off of the propellant surface, the turbulent eddy viscosity ν_t is seen to be too small to be used as a parameter in erosive burning modeling to account for turbulence transport effects. However, since the DNS for the multiscale analysis is restricted to low-to-moderate injection Reynolds numbers, conclusions cannot yet be made for those cases where Re_{inj} is large, e.g., the space shuttle booster with Re_{inj} in the range of 10^4 to 10^5.

B. Studies on Combustion of Solid Propellants

1. Quarter-Plane Geometry

A numerical study was performed by Buckmaster and Jackson [15] on the quarter-plane geometry, with the binder in the region ($x < 0$, $y < 0$), the oxidizer in the region ($x > 0$, $y < 0$), and gas for $y > 0$. An oscillating shear flow was imposed, given by

$$u = A \sin(2\pi f t) y, \qquad v = v_{\text{inj}} \tag{8}$$

where u and v are the velocity components parallel and perpendicular to the burning surface, respectively. Using a global two-step kinetics model, with a single diffusion flame and the solid phase decoupled from the fluid, it was shown that the heat flux to the surface increased in the presence of the shear flow.

A subsequent study was performed by Isfahani et al. [16] on the same geometry, but with coupling between the solid and gas, and the three-step chemistry model of Massa et al. [23], with similar results. It was shown that, for smaller dimensional shear amplitudes [$A = 3000$ (1/s)], the surface-averaged heat flux was greater when the shear is blowing AP gases over the binder and that the behavior was reversed with increased shear amplitude [$A = 10,000$ (1/s)]. For all values of shear A, integration over one period resulted in an increase in both the total averaged heat flux and the burn rate.

2. Homogeneous Propellant

The effects that velocity fluctuations may have on the combustion of homogeneous propellants were studied numerically by Zhang and Jackson [21], considering the velocity field model of Eq. (1) imposed in the gas phase. A simple one-step global kinetic scheme was considered for the combustion model. It was shown that the imposed velocity field moves the flame closer or farther away from the surface in different regions. It also stretches the flame, and it can lead to local quenching if A is sufficiently large. All this locally increases or decreases the heat flux to the surface, and thus the burn rate, leading to positive or negative erosive burning, consistent with the experimental results in Vilyunov and Dvoryashin [24].

III. Model for Current Simulations

The equations of the global three-step kinetics model, originally presented by Massa et al. [23], are briefly outlined in this section. The details of the numerical method used to solve the model equations are the same as in Massa et al. [25], where the temperature in the gas and solid phases, the species concentration in the gas phase, and the surface regression are all solved in time.

In the solid phase, the propellant is constructed as periodic cubes of spherical particles of AP in a matrix of AP/HTPB blend. These cubes or packs are generated using a numerical algorithm that targets the desired mean particle diameter, size distribution, and relative mass of AP and HTPB. The temperature in the solid follows:

$$c_p \rho_c \frac{\partial T}{\partial t} = \nabla \cdot (\lambda_c \nabla T) \tag{9}$$

where c_p is specific heat, ρ is density, λ is heat conductivity, and T is temperature. The subindex c refers to the solid or condensed phase.

The binder is, in actual experiments, composed of HTPB and fine particles of AP. However, these fine particles are too small to be resolved computationally in practical simulations. To overcome this limitation, the binder is considered as a homogeneous blend, with its thermochemical variables computed through a homogenization procedure (Chen et al. [26]).

The pyrolization of the burning surface is modeled as zero-order reactions in both the AP P_1 and binder P_2 phases:

$$P_1\text{: AP} \overset{Q_{s,1}}{\rightarrow} X \tag{10}$$

$$P_2\text{: binder} \overset{Q_{s,2}}{\rightarrow} \alpha_w X + (1 - \alpha_w) Y \tag{11}$$

with X and Y as the species concentration in the gas phase from the pyrolization of AP and HTPB, respectively; $Q_{s,1}$ and $Q_{s,2}$ as the heat of decompositions, taken as endothermic when $Q_s < 0$; and α_w as the mass fraction of AP in the homogenized binder. The local burn rate of the surface r_b, which is normal to the surface, is obtained from the pyrolysis gasification rates $\dot{m}_b$ according to

$$r_{b,1} = \frac{\dot{m}_{b,1}}{\rho_{c,1}} = A_{p,1} \exp\left(\frac{-E_{p,1}}{R_u T}\right) \tag{12}$$

$$r_{b,2} = \frac{\dot{m}_{b,2}}{\rho_{c,2}} = A_{p,2} \exp\left(\frac{-E_{p,2}}{R_u T}\right) \tag{13}$$

where $A_{p,i}$ are the pyrolysis rate constants, $E_{p,i}$ are the pyrolysis activation energies, and R_u is the universal gas constant.

The burning surface of the propellant is initially flat and coincident with the (x, z) plane. As the surface burns, its instantaneous position is determined by the single-valued function $y_s = f(x, z, t)$, which satisfies the relation

$$f_t + r_b \sqrt{1 + f_x^2 + f_z^2} = 0 \tag{14}$$

A mapping can be defined in the vertical direction as

$$\eta = y - f(x, z, t) \tag{15}$$

where now, the burning surface is located at $\eta = 0$ for all times. This mapping, which eliminates the problem of tracking the burning surface, is implemented in the numerical formulation after modifying all the equations presented here accordingly.

In the gas phase, the global-kinetics chemistry model for the combustion of AP and HTPB (Massa et al. [23]) uses three reacting species and three chemical steps according to

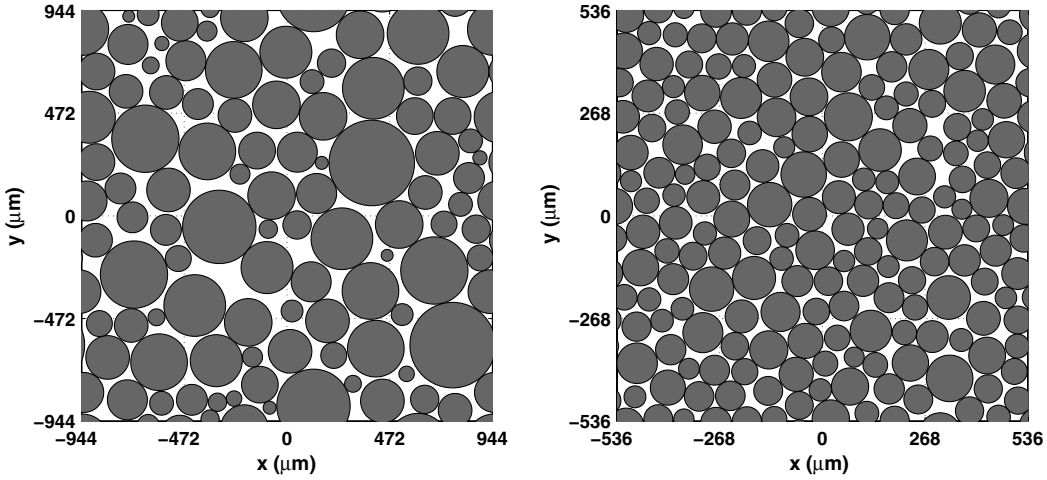

a) 200 μm **b) 90 μm**

Fig. 3 Two-dimensional packs used in study; packing fraction is 0.78.

$$R_1\colon X \overset{Q_{g,1}}{\rightarrow} Z \tag{16}$$

$$R_2\colon \beta X + Y \overset{Q_{g,2}}{\rightarrow} \text{final products} \tag{17}$$

$$R_3\colon \beta Z + Y \overset{Q_{g,3}}{\rightarrow} \text{final products} \tag{18}$$

where X, Y, and Z are the model species; β is the mass-based stoichiometric ratio of AP over HTPB; and $Q_{g,j}$ are the heats of reaction, where $j = 1, 2, 3$ specifies the reaction number. These reactions account for the monopropellant premixed flame R_1 and the primary and final diffusion flames (R_2, R_3) of the Beckstead–Derr–Price model model [27]. The reaction rates R_j are determined from

$$R_1 = D_1 P_0^{n_1} X \exp\left(\frac{-E_1}{R_u T}\right) \tag{19}$$

$$R_2 = D_2 P_0^{n_2} X^{3.3} Y^{0.4} \exp\left(\frac{-E_2}{R_u T}\right) \tag{20}$$

$$R_3 = D_3 P_0^{n_3} Y Z \exp\left(\frac{-E_3}{R_u T}\right) \tag{21}$$

with D_j as the reaction constants, P_0 as pressure, n_j as the pressure exponents, and E_j as the activation energies. The temperature and X species fields are determined from

$$\rho\left(\frac{\partial T}{\partial t} + \mathbf{u}\cdot\nabla T\right) = \nabla\cdot\left(\frac{\lambda_g}{c_p}\nabla T\right) + \frac{\dot{\omega}_T}{c_p} \tag{22}$$

$$\rho\left(\frac{\partial X}{\partial t} + \mathbf{u}\cdot\nabla X\right) = \nabla\cdot\left(\frac{\lambda_g}{c_p}\nabla X\right) + \frac{\dot{\omega}_X}{c_p} \tag{23}$$

with analogous equations for the evolution of the Y and Z fields. Here, $\dot{\omega}_T$ is the rate of heat release due to combustion, and $\dot{\omega}_X$ ($\dot{\omega}_Y, \dot{\omega}_Z$) is the rate of change of X (Y, Z) due to all reactions. Thus,

$$\dot{\omega}_T = \sum_{j=1}^{3} Q_{g,j} R_j, \qquad \dot{\omega}_X = -R_1 - \beta R_2 \tag{24}$$

$$\dot{\omega}_Y = -R_2 - R_3, \qquad \dot{\omega}_Z = R_1 - \beta R_3 \tag{25}$$

The gas density is computed from the equation of state for a perfect gas:

$$P_0 = \frac{\rho R_u T}{\text{MW}} \tag{26}$$

where MW is the molecular weight, taken as constant for all species.

In two dimensions, Eq. (1) is used as the imposed velocities. In three dimensions, the velocities (u, v, w) are imposed, considering an Oseen approximation in the y direction and a constant shear flow in the x direction. Thus, $u = A\eta$, $\rho_g v =$ constant, and $w = 0$. The steady shear flow is a simplification from that of Eq. (1) that allows us to evaluate the effect of the mean shear flow in erosive burning for the current model. It is expected that the erosive burning effect will still be evident, since the burn rate is governed mainly by the PDF.

The connection conditions at the surface are derived from the continuity of temperature and normal mass flux and the conservation of energy and species across the surface:

$$[T] = 0 \tag{27}$$

$$[\rho\mathbf{n}\cdot\mathbf{v}] = 0 \tag{28}$$

$$[\lambda\mathbf{n}\cdot\nabla T] = -\rho_c r_b Q_s \tag{29}$$

$$\left[\frac{\lambda}{c_p}\mathbf{n}\cdot\nabla Y_i\right] = \rho_c r_b [Y_i] \tag{30}$$

where $[\cdot] = (\cdot)_g - (\cdot)_c$ is a jump operator across the surface, $\mathbf{n}$ is the unit vector normal to the surface with sense toward the gas, and Y_i

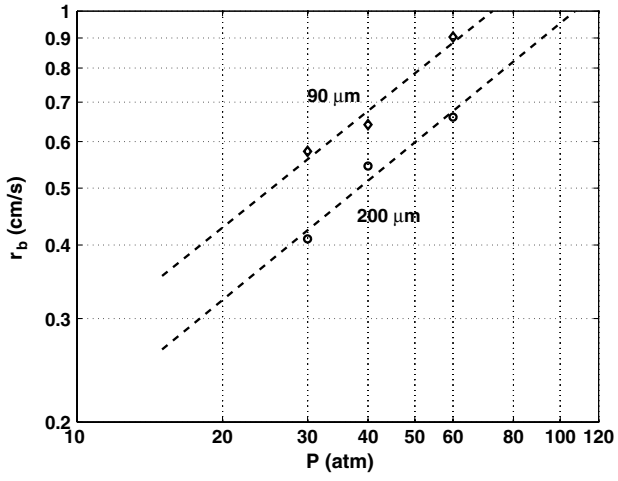

Fig. 4 Burn rates as a function of pressure; no shear.

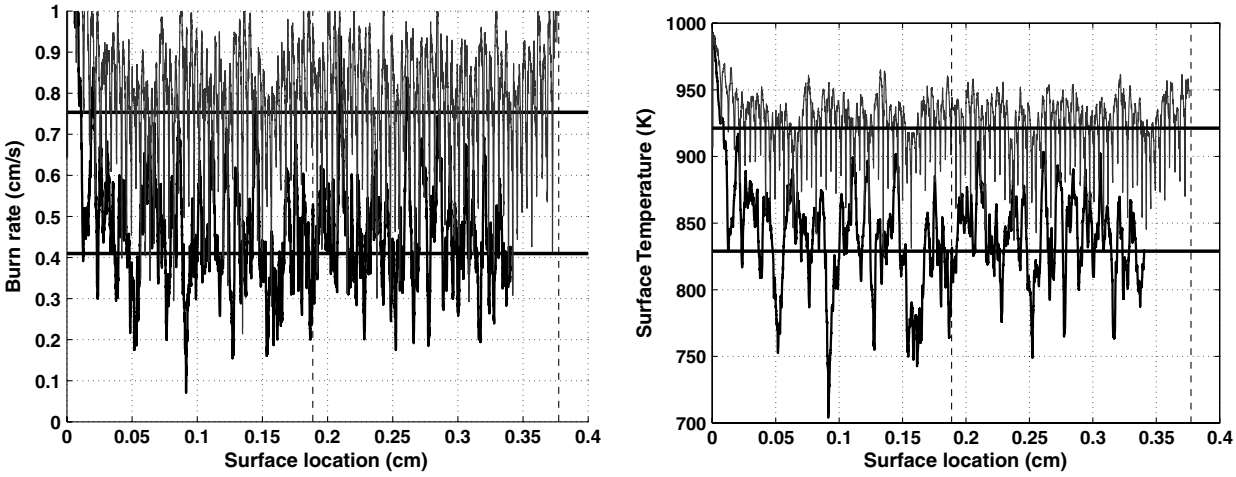

a) b)

Fig. 5 Surface-averaged a) burn rate and b) temperature as a function of averaged surface location for 200 μm pack and for shear amplitudes of 0 (thick) and 1e − 4 1/s (thin).

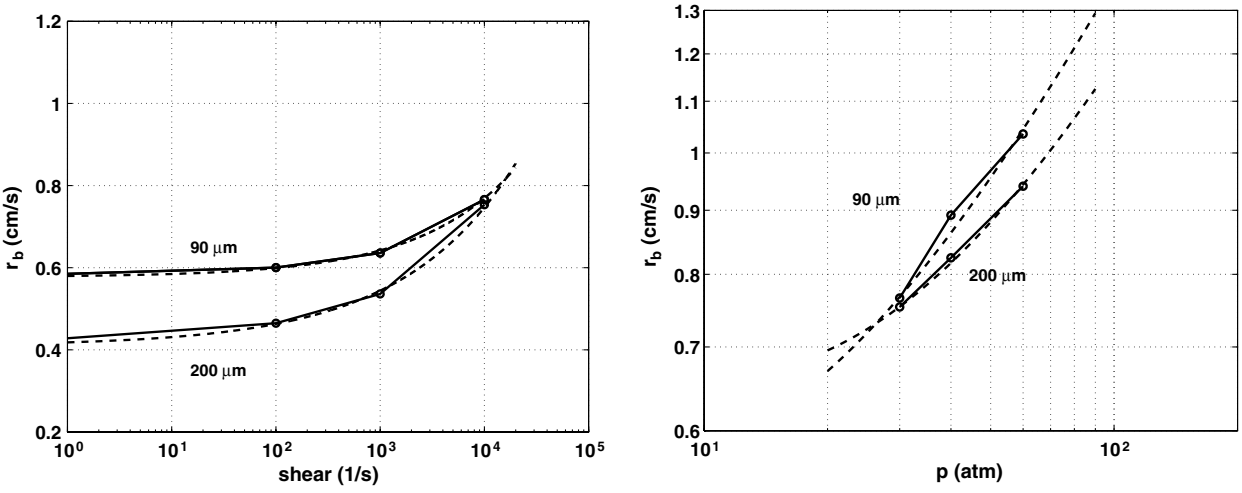

a) b)

Fig. 6 Burn rates as a) a function of shear rate at a pressure of 30 atm, and b) a function of pressure at a fixed shear amplitude of 10(4) 1/s. The dashed curves correspond to the fits given by Eq. (33). In both cases, $f = 100$ Hz.

represents any of X, Y, or Z. For all the cases studied, the thermochemical parameters of AP and HTPB are taken to be the same as in Massa et al. [23].

IV. Erosive Burning Results

A. Results for Two-Dimensional Packs

We first present results for two-dimensional packs of AP/HTPB using the velocity field suggested by the multiscale analysis.

For heterogeneous propellants, the multiscale analysis suggests that the shear near the propellant surface is only time dependent, since the spatial scales are much larger than a typical AP particle diameter. We therefore model the shear via $u = A\sin(2\pi ft)\eta$, where A is the shear rate, f is the frequency, t is the time, and η is the coordinate in the normal direction to the propellant surface. Figure 3 shows the packs used in this study. Two packs are considered: a 200 and a 90 μm pack. For each pack, a distribution about the mean is used to represent typical distributions found in real propellants. The packing fraction is fixed at 78%, and the void spaces represent the binder region. The packs are periodic in a square of length $2L$. Corresponding burn rates as a function of pressure are plotted in Fig. 4 in the absence of shear. The symbols are the simulation data, and the dashed line is a least-squares fit through the data assuming

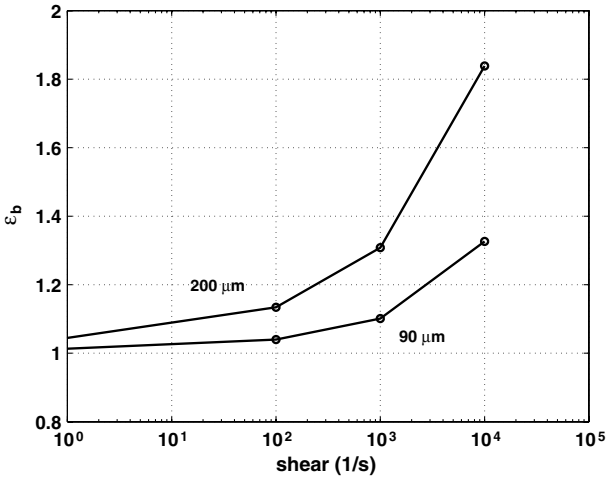

Fig. 7 Erosive burning rate coefficient, $\epsilon_b = r_b/r_0$, as a function of shear rate; pressure is 30 atm and $f = 100$ Hz.

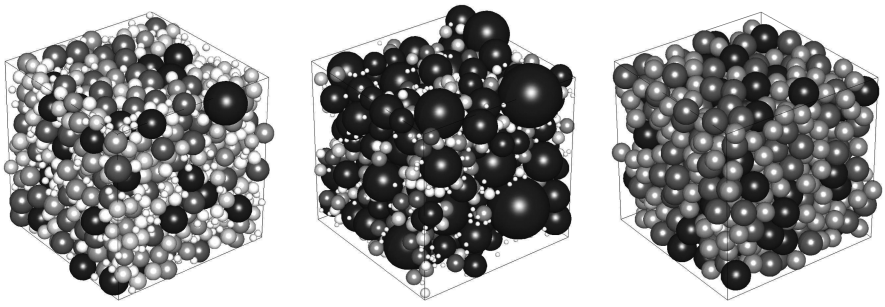

a) M90 b) M200 c) M400

Fig. 8 Three-dimensional packs used in study. The volume fraction (total AP volume/pack volume) of each pack is 0.766. The particle number and length scale of each pack are as follows: 90 μm: (2001, 602 μm); 200 μm: (1200, 1027 μm); and 400 μm: (650, 3201 μm).

$$r_0 = ap^n, \qquad a = \begin{cases} 0.0429 \\ 0.0595 \end{cases}$$
$$n = \begin{cases} 0.6737 & 200\ \mu\text{m pack} \\ 0.6590 & 90\ \mu\text{m pack} \end{cases} \tag{31}$$

To examine the effect of an imposed time-periodic shear, we plot the burn rate and the corresponding surface temperature as a function of surface location for the 200 μm pack in Fig. 5 for two different shear amplitudes and for a pressure of 30 atm and an f of 100 Hz. Roughly two periods of the pack are shown; the vertical dashed lines correspond to a period of approximately 1888 μm. Also shown as horizontal solid lines are the corresponding burn rate and temperature means. Note that, as the shear amplitude increases, the average burn rate and average surface temperature also increase. This observation of erosive burning effect in the presence of shear can possibly be explained by appealing to the numerical results of the quarter-plane geometry [15], where in Fig. 11 of [15], the integrated heat flux and the maximum reaction rate are plotted as a function of $(\omega t)/\pi$, where the velocity is given by $u = kx\sin(\omega t)$. Note from the figure that, in the first half of the period, when the shear is blowing AP gases over the binder, the integrated heat flux is essentially unaffected, whereas the maximum reaction rate is significantly increased. But upon reversal, in the second half of the period, when the shear is blowing binder gases over the AP, the integrated heat flux is significantly increased, whereas the maximum reaction rate is relatively unchanged. This makes it clear that the maximum reaction rate, a pointwise value, is not a useful indicator for the integrated heat flux, a volumetric quantity. Thus, in Fig. 6 of [15], we see that the area over which the edge flame has a significant reaction rate is much bigger at the three-quarter period than it is at the one-quarter period, and it is this area increase that is responsible for the increase in the integrated heat flux.

Figure 6a shows the mean burn rate as a function of shear amplitude at a pressure of 30 atm for the two packs, while Fig. 6b plots the burn rate as a function of pressure for a fixed shear amplitude of $A = 10^4$ 1/s. Note that the burn rate at $A = 0$ for the 90 μm pack is larger than the burn rate for the 200 μm pack, a particle size effect consistent with experimental observations [28]. This is because decreasing the AP particle diameter increases the number of PDFs, thereby increasing the nominal burn rate.

In modeling the experimental work of Furfaro [7], Wang [29] developed an empirical-based erosive burning model based on the Reynolds analogy. The Reynolds analogy postulates the existence of a relationship between heat transfer and friction, and it leads to the following equation:

$$r_b - r_0 = c_1 \left|\frac{\partial u}{\partial y}\right|^{c_2} p^{c_3} \tag{32}$$

This expression is similar to the one presented in Wang [29] [see Eqs. (7–10)]. Our expression takes into account a slight pressure dependence, due to the temperature dependence of the thermal conductivity [Eq. (6)]. Using the data of Fig. 6, we solve the least-squares problem for the Reynolds analogy Eq. (32), and we obtain the following fits:

$$200\ \mu\text{m: } r_b - r_0 = 0.0138A^{0.4562}p^{-0.3025}$$
$$90\ \mu\text{m: } r_b - r_0 = 0.0238A^{0.3705}p^{-0.3663} \tag{33}$$

with $A = |\frac{\partial u}{\partial y}|$. Note that the pressure exponent in the Reynolds analogy fit is negative. The numerical fits given by Eq. (33) are shown as dashed curves in Fig. 6. Since we have only limited data, and since two-dimensional packs are only meant to be representative of the trends, we did not attempt a fit that included particle size effect. Such a fit is more properly done when examining three-dimensional packs.

Figure 7 plots the erosive burning rate coefficient, $\epsilon_b = r_b/r_0$, as a function of shear at a pressure of 30 atm. Note that when normalized by the nominal burn rate r_0, the 200 μm pack experiences a greater erosive burning effect than the 90 μm pack. This is consistent with experimental observations that show that packs with larger AP particle sizes have a larger erosive coefficient than packs containing smaller AP particle sizes [6]. Note that, as the AP particle size decreases, the edge flame effectively disappears and a premixed region develops that supports a one-dimensional flame; see Gross and Beckstead [30,31] for a discussion of the particle size effect on the combustion dynamics of the edge flame. In this case, shear that is parallel to the surface would have less effect on a quasi-one-dimensional flame that is parallel to the surface. It would then be more adequate to use Eq. (1), considering a finite λ to account for the spatial variation of the velocity field.

An explanation[¶] of particle size effect on erosive burning is sought through the observation of the damping effect of large nominal burn rate. Since the 90 μm pack has a larger nominal burn rate r_0, as we just showed in Fig. 6a, erosive burning is less pronounced than for the 200 μm pack. This is confirmed by a numerical experiment in which the nominal burn rate of the 200 μm pack is artificially increased by increasing $A_{p,1}$ and $A_{p,2}$ in Eqs. (12) and (13) to match that for the 90 μm pack. Erosive simulations then show that almost the same value of the normalized burn rate ϵ_b as that for the 90 μm pack is obtained.

Table 2 Pack parameters

Parameter	M90	M200	M400
Length, μm	602	1027	3201
Number of particles	2001	1200	650
Minimum particle size, μm	25.7	26.7	230
Fine AP volume/blend volume	0.263	0.219	0.328

[¶]This was suggested in the peer review of the current paper by one of the anonymous reviewers.

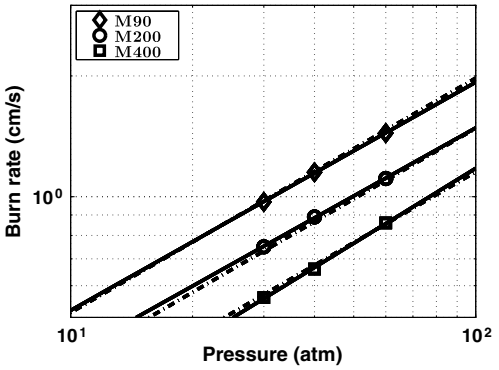

Fig. 9 Burn rate as a function of pressure for different packs; no shear.

B. Results for Three-Dimensional Monomodal Packs

Three monomodal packs are considered to assess the particle size effect on erosive burning for the proposed shear model. The three-dimensional packs are shown in Fig. 8, and relevant information of their characteristics is presented in Table 2. In all cases, the mass ratio of AP to HTPB is the stoichiometric ratio 88:12. Therefore, the ratio of the volume of AP over the total volume of the pack is 0.766.

The burn rates are obtained for a range of pressures ($p = 30$, 40, and 60 atm) and shear rates ($A = 0$, 10^3, and 10^4 (1/s)). Each burn rate is computed as the average in space and time over a period in the length of the pack and after the initial temperature transient in the simulation. The results for the reference case of no shear at different pressures are shown in Fig. 9. It is seen that, as expected, the burn rate increases with pressure. Also, the burn rate is higher for lower mean particle diameter, a well-known particle size effect of AP/HTPB-based propellants, where the burn rate is influenced mainly by the heat generated and transferred to the surface by the PDF.

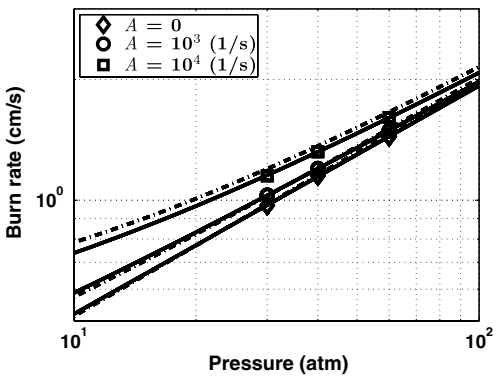

a) Surface-averaged burn rate vs pressure, M90

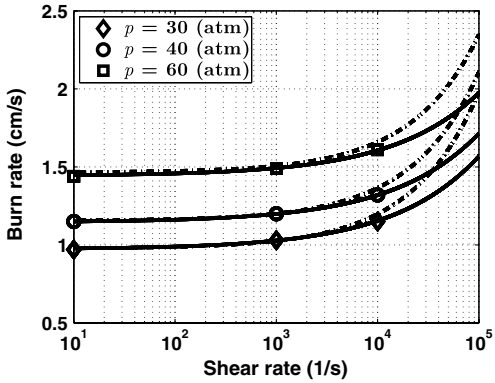

b) Surface-averaged burn rate vs shear, M90

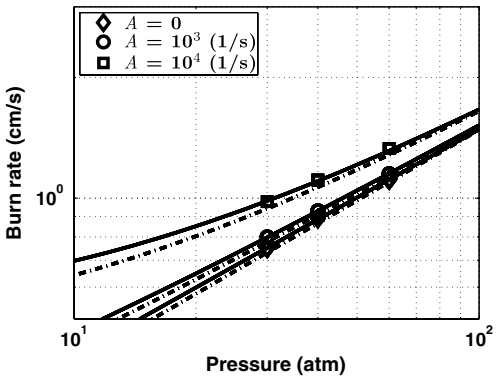

c) Surface-averaged burn rate vs pressure, M200

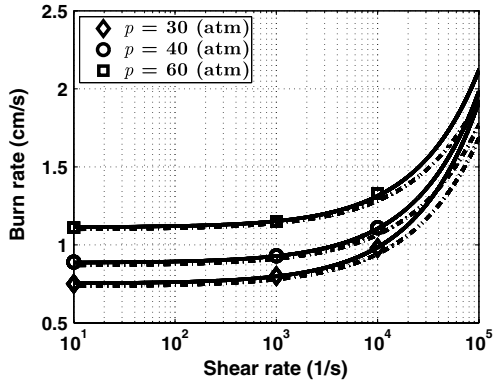

d) Surface-averaged burn rate vs shear, M200

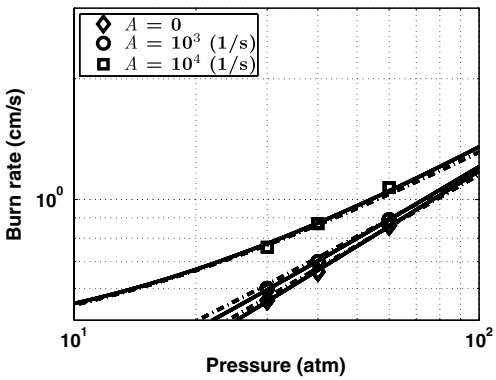

e) Surface-averaged burn rate vs pressure, M400

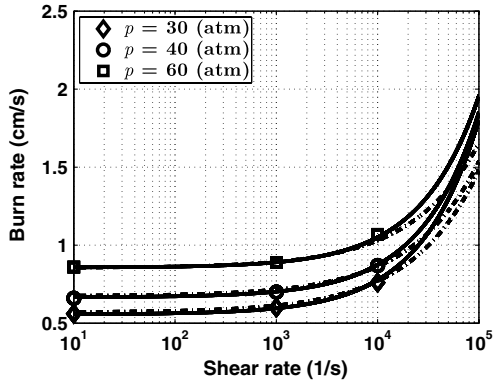

f) Surface-averaged burn rate vs shear, M400

Fig. 10 Burn rate for different packs: a, c, and e) burn rate vs pressure for packs M90, M200, and M400, respectively; and b, d, and f) burn rate vs shear for packs M90, M200, and M400, respectively.

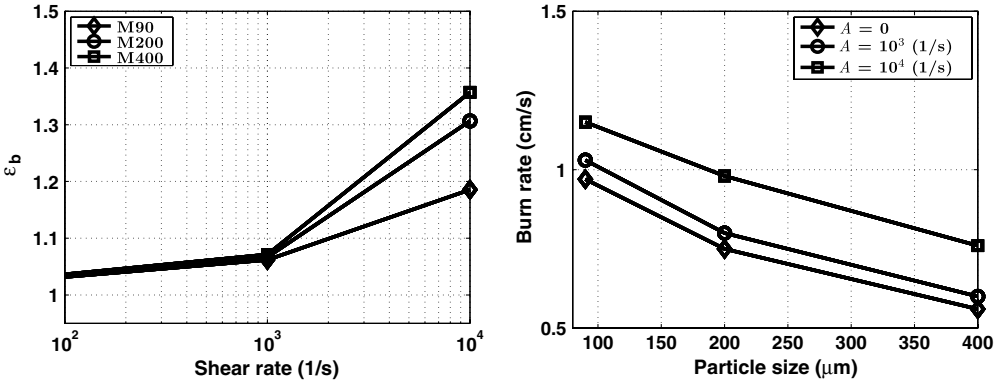

a) Erosive burning coefficient vs shear

b) Burn rate as a function of mean particle size

Fig. 11 Erosive burning coefficient and particle size effect at $p = 30$ atm: a) erosive rate as a function of shear rate for different packs and b) burn rate as a function of mean particle size for different shear rates.

Figure 10 shows the burn rates for the different packs, where Figs. 10a, 10c, and 10e show the variation in burn rate with pressure for different shear rates, while Figs. 10b, 10d, and 10f show the variation with shear for different values of pressure. It is seen that, for each pack, the burn rate increases with both pressure and shear rate.

In Fig. 11, the results at the selected pressure of $p = 30$ atm. are presented in terms of the erosive burning rate coefficient as a function of shear rate (Fig. 11a) and burn rate vs mean particle diameter (Fig. 11b). From Fig. 11a, it is seen that, just as in two dimensions, when each burn rate is normalized by its respective no shear value, the erosive burning rate coefficient increases for a fixed shear rate as the AP mean particle diameter increases. This result is consistent with experimental observations [6]. Furthermore, from Fig. 11b, it is noted that the burn rate decreases as the mean particle diameter increases, a morphology effect also consistent with experimental results [6].

Similar to the two-dimensional results, a Reynolds analogy argument is used to relate the burn rate to the shear; that is,

$$r_b(A, p; D_p) - r_0(p; D_p) = c_1 A^{c_2} p^{c_3}, \qquad r_0(p; D_p) = a p^n \quad (34)$$

where $r_0(p; D_p)$ is the burn rate for no shear; $r_b(p, A; D_p)$ is the burn rate with shear; p is the pressure; A is the shear rate; and a, n, c_1, c_2, and c_3 are empirical constants. D_p is used to make explicit the dependence of the empirical constants enumerated before on the pack parameters, characterized mainly by the mean particle diameter.

To obtain the constants for the different packs using the current results, we solve a nonlinear least-squares problem using the data of Fig. 10. The results obtained are summarized in Table 3. Note that the pressure exponent in the Reynolds analogy fit is negative, consistent with the two-dimensional results presented earlier and with the quarter-plane geometry study by Isfahani et al. [16]. The numerical fits given by Eq. (34) are shown as the solid curves in Fig. 10.

An alternative fit is also considered, where the particle diameter is weighted explicitly in the fitting equation as

$$r_b(A, p, D_p) - r_0(p, D_p) = c_1 A^{c_2} p^{c_3} D_p^{c_4} \quad (35)$$

$$r_0(p, D_p) = a p^n D_p^m \quad (36)$$

We can draw similar conclusions to the previous case, where a different equation is considered for each mean particle diameter. The results for this fit are presented in the last column of Table 3 and in dashed–dotted lines in Figs. 9 and 10.

V. Comparison with Experiments

In this section, we present the erosive burning response of a bimodal pack of AP/HTPB, composed of AP particles of mean diameters of 200 μm (68.35%) and 90 μm (13.65%), where the numbers in parentheses are the mass fraction of each cut in the propellant. The aim of this set of results is to compare against the experimental results reported by King [6] using a propellant of similar characteristics.

The results of these runs are presented in Fig. 12, where it is seen that the trend and results in the burn rate against pressure obtained with our model simulations are, considering the simplicity of the current model, in good agreement with experiments, with the nominal burn rates higher than in experiments, and the erosive burning rate lower than in experiments. We note, however, the difficulty in comparing against the published results under crossflow, both because of the scatter in the experimental results and the lack of precise information regarding the shear rate of the velocity field at the burning surface. For example, the crossflow velocity of 335 m/s in King's results [6] used in Fig. 12 has an uncertainty of 40 m/s. As a reference, the curves of the erosive burning model by King [6] (dashed and dashed–dotted curves in Fig. 12, where the dashed–dotted curve corresponds to a crossflow velocity of 210 m/s and a dashed curve corresponds to 305 m/s) are also included, where it is seen that the predicted slopes of the curves for King's model are steeper than those obtained in the current work.

Regarding the results presented in Fig. 12b, in order to compare numerical and experimental results, it is necessary to relate the crossflow velocity of King's experiments [6] with the shear rate at the surface. Although it is not possible to obtain the actual shear rate in experiments, since the details of the flowfield for the particular apparatus used by King are not known, an estimate of the order of magnitude can be obtained as follows. The experimental apparatus used by King consisted, in the test section, of a channel of 1.9 cm of width, 30 cm in length of burning propellant, and 1.9 cm in initial

Table 3 Reynolds analogy parameters

Parameter	M90	M200	M400	Global fit
a	0.1404	0.1104	0.0674	0.6785
n	0.5690	0.5642	0.6211	0.5848
m				−0.3611
c_1	2.7966×10^{-3}	0.7483×10^{-3}	0.3932×10^{-3}	1.3290×10^{-3}
c_2	0.513	0.701	0.755	0.656
c_3	−0.161	−0.212	−0.184	−0.186
c_4				−0.0664

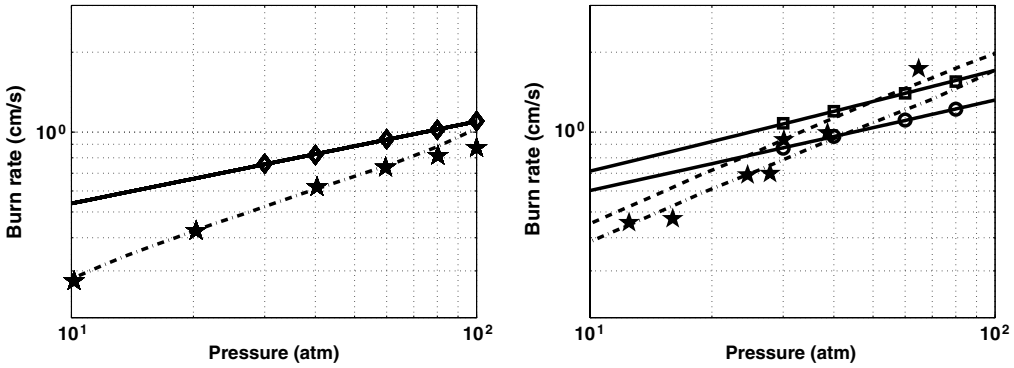

a) No shear flow **b) With shear flow**

Fig. 12 Comparison of burn rates with experiments by King [6]. King's results (stars) and numerical results: $A = 0$ (diamonds), $10^3 s^{-1}$ (circles), and 10^4 s^{-1} (squares).

height, which increased to 4.45 cm as the burning propellant receded [6]. As a first approximation to the order of magnitude of the shear rate, we consider the velocity profile given by the Culick solution for a porous rectangular channel of height $2h$ with constant injection velocity on both sides and incompressible flow, which in dimensional form is

$$U = v_{\text{inj}} \frac{\pi}{2} \frac{x}{h} \cos \frac{\pi y}{2h}, \qquad V = -v_{\text{inj}} \sin\left(\frac{\pi y}{2h}\right)$$
$$-h < y < h, \qquad x > 0 \tag{37}$$

The velocity at the centerline is $U_c = v_{\text{inj}} \frac{\pi}{2} \frac{x}{h}$, and the shear rate at the surface is $U_{,y} = v_{\text{inj}} (\frac{\pi}{2h})^2 x$. Then, the shear rate at the surface can be expressed in terms of the velocity at the centerline as $|\frac{\partial U}{\partial y}|_{y=\pm h} = U_c \frac{\pi}{2h}$. For a centerline velocity of 335 m/s, the shear rate is approximately 2×10^4 s^{-1}. We note that this calculation serves only as a rough estimate of the order of magnitude of the shear rate, since there are many factors that are not taken into account like turbulence effects, compressibility, and the particular evolution of the flow profile in the actual experimental apparatus. As it was shown by Zhang and Jackson [20], turbulence can add a strong harmonic shear rate at the propellant surface.

VI. Conclusions

The effects of an imposed shear flow on the burning rate of both two- and three-dimensional heterogeneous packs were investigated. The shear model is based on a multiscale study of the injection-driven turbulent flowfield by Zhang and Jackson [20]. Three important outcomes of the multiscale analysis are relevant here:

1) There is a region at the propellant surface where a space- and time-dependent shear flow exists. The results suggest a model for the velocity field near the propellant surface that can be incorporated into erosive burning simulations. This has been used in the previous study of homogeneous propellants [21] and now here in the study of multidimensional packs of AP and binder. Parameters for the wavelength, frequency, and amplitude are determined from the multiscale results.

2) As noted by Buckmaster and Jackson [15], the effect of the shear flow on the PDF may be a main factor in the erosive burning effect of heterogeneous AP/HTPB solid propellants. The turbulent eddy viscosity is found to be smaller than previously assumed near the propellant surface, making it less likely for the variation of turbulent transport properties near the PDF to have any effect on erosive burning. Any erosive burning model that incorporates a model for the turbulent eddy viscosity might need to be reexamined in light of our findings.

3) There exists a universal curve between the nondimensional crossflow velocity and the total (mean plus rms) nondimensional shear. For a particular motor geometry, this curve can be used as a guide for determining the potential effect of erosive burning.

Numerical simulations using an imposed shear flow qualitatively reproduce the observations found in experiments for packs of different mean particle diameter and at different pressures. The key concern raised by the work of Buckmaster and Jackson [15] is whether or not the nonlinear effect of the oscillating shear averages out when applied to a heterogeneous pack; the simulations indicate that this is not the case.

The numerical burn rate trends are in qualitative agreement with those observed in experiments. That is, higher burn rates are observed as the shear rate increases. The effect of differences in mean particle diameter of the pack was noted as well, where the erosive burning rate coefficient was larger for packs with larger mean particle diameter: the pressure and shear rate being the same. A Reynolds analogy model is used to fit the data, leading to an erosive burning rate model that can be incorporated in full rocket chamber simulations.

A comparison with experiments by King [6] was also performed, where it was shown that the results obtained compare qualitatively well after considering an estimate of the shear rate in the experimental apparatus using the Culick solution for a transpired incompressible duct.

Acknowledgments

This work was supported by the U.S. Department of Energy, through the University of California under subcontract B523819, and by the NASA Constellation University Institutes Project under grant NCC3-989, through the University of Maryland with subcontract Z634015 to the University of Illinois at Urbana–Champaign, with Claudia Meyer as the project manager. The use of the Turing cluster, maintained and operated by the Computational Science and Engineering Program at the University of Illinois, is gratefully acknowledged.

References

[1] Green, L., "Erosive Burning of Some Composite Solid Propellants," *Jet Propulsion*, Vol. 24, No. 1, 1954, pp. 9–15.

[2] Marklund, T., and Lake, A., "Experimental Investigation of Propellant Erosion," *ARS Journal*, Vol. 30, No. 2, 1960, pp. 173–178.

[3] Gordon, J. C., Duterque, J., and Lengelle, G., "Solid Propellant Erosive Burning," *Journal of Propulsion and Power*, Vol. 8, No. 4, 1992, pp. 741–747. doi:10.2514/3.23544

[4] Bulgakov, V. K., Karpov, A. I., and Lipanov, A. M., "Numerical Studies of Solid Propellant Erosive Burning," *Journal of Propulsion and Power*, Vol. 9, No. 6, 1993, pp. 812–818. doi:10.2514/3.23694

[5] Gordon, J. C., Duterque, J., and Lengelle, G., "Erosive Burning in Solid Propellant Motors," *Journal of Propulsion and Power*, Vol. 9, No. 6, 1993, pp. 806–811. doi:10.2514/3.23693

[6] King, M. K., "Erosive Burning of Solid Propellants," *Journal of Propulsion and Power*, Vol. 9, No. 6, 1993, pp. 785–805.

doi:10.2514/3.23692
[7] Furfaro, J. A., "Erosive Burning Study Utilizing Ultrasonic Measurement Techniques," AIAA Paper 2003-4806, 2003.
[8] Krishnan, S., and Rajesh, K. K., "Erosive Burning of Ammonium Perchlorate/Hydroxyl-Terminated-Polybutadiene Propellants Under Supersonic Crossflows," *Journal of Propulsion and Power*, Vol. 19, No. 4, 2003, pp. 623–631.
doi:10.2514/2.6150
[9] Landsbaum, E. M., "Erosive Burning of Solid Rocket Propellants: A Revisit," *Journal of Propulsion and Power*, Vol. 21, No. 3, 2005, pp. 470–477.
doi:10.2514/1.5234
[10] Moss, J., Heister, S., and Linke, K., "Experimental Program to Assess Erosive Burning in Segmented Solid Rocket Motors," AIAA Paper 2007-5782, 2007.
[11] Cai, W., Thakre, P., and Yang, V., "A Model of AP/HTPB Composite Propellant Combustion in Rocket-Motor Environments," *Combustion Science and Technology*, Vol. 180, No. 12, 2008, pp. 2143–2169.
doi:10.1080/00102200802414915
[12] Cai, W., Thakre, P., and Yang, V., "Transient Combustion Response of AP/HTPB Composite Propellant to Acoustic Oscillations in a Rocket Motor," *Combustion Science and Technology*, Vol. 181, No. 4, 2009, pp. 597–617.
doi:10.1080/00102200802693781
[13] McDonald, B. A., and Menon, S., "Direct Numerical Simulation of Solid Propellant Combustion in Crossflow," *Journal of Propulsion and Power*, Vol. 21, No. 3, 2005, pp. 460–469.
doi:10.2514/1.10049
[14] Lenoir, J. M., and Robillard, G., "A Mathematical Method to Predict the Effects of Erosive Burning in Solid Propellant Rockets," *Proceedings of the Sixth Symposium (International) on Combustion*, Reinhold, New York, 1957, pp. 663–667.
[15] Buckmaster, J., and Jackson, T. L., "The Effects of Time-Periodic Shear on a Diffusion Flame Anchored to a Propellant," *Combustion and Flame*, Vol. 120, Nos. 1–2, 2000, pp. 211–221.
doi:10.1016/S0010-2180(99)00088-7
[16] Isfahani, A. H. G., Zhang, J., and Jackson, T. L., "The Effects of Turbulence-Induced Time-Periodic Shear on a Flame Anchored to a Propellant," *Combustion and Flame*, Vol. 156, No. 5, 2009, pp. 1084–1098.
doi:10.1016/j.combustflame.2008.12.009
[17] Buckmaster, J., Jackson, T. L., and Yao, J., "An Elementary Discussion of Propellant Flame Geometry," *Combustion and Flame*, Vol. 117, No. 3, 1999, pp. 541–552.
doi:10.1016/S0010-2180(98)00116-3
[18] Burke, S. P., and Schumann, T. E. W., "Diffusion Flames," *Industrial and Engineering Chemistry*, Vol. 20, No. 10, 1928, pp. 998–1004.
doi:10.1021/ie50226a005
[19] Venugopal, P., Moser, R. D., and Najjar, F. M., "Direct Numerical Simulation of Turbulence in Injection Driven Plane Channel Flows," *Physics of Fluids*, Vol. 20, No. 10, 2008, Paper 105103.
doi:10.1063/1.2963137
[20] Zhang, J., and Jackson, T. L., "Direct Numerical Simulation of Turbulence in Injection Driven Three-Dimensional Cylindrical Flows," *Journal of Fluid Mechanics*, Vol. 670, 2011, pp. 176–203.
[21] Zhang, J., and Jackson, T. L., "A Model for Erosive Burning of Homogeneous Propellants," *Combustion and Flame*, Vol. 157, No. 2, 2010, pp. 397–407.
doi:10.1016/j.combustflame.2009.09.008
[22] Spalart, P., "Direct Simulation of a Turbulent Boundary Layer up to $Re_\theta = 1410$," *Journal of Fluid Mechanics*, Vol. 187, 1988, pp. 61–98.
doi:10.1017/S0022112088000345
[23] Massa, L., Jackson, T. L., and Buckmaster, J., "New Kinetics for a Model of Heterogeneous Propellant Combustion," *Journal of Propulsion and Power*, Vol. 21, No. 5, 2005, pp. 914–924.
doi:10.2514/1.2433
[24] Vilyunov, V. N., and Dvoryashin, A. A., "An Experimental Investigation of Erosive Burning Effects," *Combustion, Explosion, and Shock Waves*, Vol. 7, No. 1, 1973, pp. 38–42.
doi:10.1007/BF00748911
[25] Massa, L., Jackson, T. L., and Short, M., "Numerical Solution of Three-Dimensional Heterogeneous Solid Propellants," *Combustion Theory and Modelling*, Vol. 7, No. 3, 2003, pp. 579–602.
doi:10.1088/1364-7830/7/3/308
[26] Chen, M., Buckmaster, J., Jackson, T. L., and Massa, L., "Homogenization Issues and the Combustion of Heterogeneous Solid Propellants," *Proceedings of the Combustion Institute*, Vol. 29, No. 2, 2002, pp. 2923–2929.
doi:10.1016/S1540-7489(02)80357-1
[27] Beckstead, M., Derr, R. L., and Price, C. F., "A Model of Composite Solid-Propellant Combustion Based on Multiple Flames," *AIAA Journal*, Vol. 8, No. 12, 1970, pp. 2200–2207.
doi:10.2514/3.6087
[28] Miller, R. R., "Effects of Particle Size on Reduced Smoke Propellant Ballistics," AIAA Paper 1982-1096, 1982.
[29] Wang, Q., "Development of Erosive Burning Models for CFD Predictions of Solid Rocket Motor Internal Environment," AIAA Paper 2003-4809, 2003.
[30] Gross, M. L., and Beckstead, M. W., "Diffusion Flame Calculations for Composite Propellants Using a Vorticity-Velocity Formulation," *Journal of Propulsion and Power*, Vol. 25, No. 1, 2009, pp. 74–82.
doi:10.2514/1.36360
[31] Gross, M. L., and Beckstead, M. W., "Diffusion Flame Calculations for Composite Propellants Predicting Particle-Size Effects," *Combustion and Flame*, Vol. 157, No. 5, 2010, pp. 864–873.
doi:10.1016/j.combustflame.2009.09.004

S. Son
Associate Editor